Variation of Elastic Properties of Responsive Polymer Nanotubes

Sadia Radji,*,† Halima Alem,‡ Sophie Demoustier-Champagne,§ Alain M. Jonas,§ and Stéphane Cuenot†

Institut des Matériaux Jean Rouxel (IMN), Université de Nantes, 2, Rue de la Houssinière, 44322 Nantes cedex 3, France, Laboratoire de Chimie Physique Macromoléculaire, UMR CNRS-INPL 7568, Nancy Université, ENSIC, 1 rue Grandville - BP451, 54001 Nancy cedex 1, France, and Institute of Condensed Matter and Nanosciences - Bio & Soft Matter (IMCN/BSMA), Université catholique de Louvain Place Croix du Sud, 1, B-1348 Louvain-la-Neuve, Belgium

Received: October 13, 2009; Revised Manuscript Received: February 8, 2010

The mechanical properties of thermo-responsive nanoribbons made of poly(*N*-isopropylacrylamide)-*block*-poly(ethylene terephthalate) (PNIPAM-*b*-PET) have been investigated. The nanoribbons are produced by grafting PNIPAM chains from the walls of nanopores of PET track-etched membranes, by dissolving the membranes. The swelling ratio and elastic modulus of the nanoribbons are evaluated as a function of polymer chain length and temperature, from atomic force microscopy (AFM) images and using the thermodynamic theory of swelling. Whereas the elastic properties of nanoribbons are similar to those of PNIPAM gels and brushes when the PNIPAM chain length is low, they increase by 2 orders of magnitude when the chain length becomes similar to the diameter of the nanopores used to synthesize them. This indicates that PNIPAM brushes synthesized in severe conditions of confinement are strongly cross-linked, either due to irreversible trapping of entanglements, or chemical cross-linking occurring in the dense reaction medium. This provides a way to modulate mechanical properties of soft nanostructures, by playing with the degree of confinement of the chains during synthesis.

1. Introduction

Over the past 10 years, the investigation of the physical properties of numerous nanomaterials has been the subject of intense research efforts from both theoretical and experimental perspectives.[1] Detailed knowledge of material properties is essential to determine material functionality and application domains. In particular, knowledge and understanding of mechanical properties are of considerable interest to successfully integrate these nanometer-sized objects as building blocks into emerging devices (circuit interconnects, nanoelectromechanical systems (NEMS), nanocomposite strengtheners).[2,3] In this context, atomic force microscopy (AFM) has emerged as a unique and versatile tool for the experimental evaluation of elastic properties of various one-dimensional nano-objects. Indeed, AFM-based methods have been developed to measure the elastic modulus of carbon nanotubes,[4–7] metallic nanowires,[8,9] and polymer nanotubes,[10] to quote only a few.

Because of their structure change upon applying an external stimulus, responsive polymers are ideal candidates to probe the relationship between structure and mechanical properties. Indeed, this extraordinary class of polymers is well-known for showing unique, rapid, and "switchable" structure−property changes depending on the application of various external stimuli, such as pH, electric field, temperature.[11–13] Among them, poly(*N*-isopropylacrylamide) (PNIPAM) is probably one of the most studied responsive polymers due to its reversible phase transition behavior with temperature: in water, the swollen polymer matrix shrinks as the temperature is increased above the lower critical solution temperature (LCST).[14–16] On the basis of this unique property, various applications have been developed in optical, chemical, and environmental areas.[17,18] Additionally, as the PNIPAM transition temperature (∼32 °C) is close to the human body temperature, potential applications in the biomedical field (drug delivery, tissue engineering, biosensing, etc.) are currently being investigated.[19,20] For a large number of these applications and also for the integration of PNIPAM into nanometer-sized devices, such as bio-NEMS or biomedical devices, it is crucial to know exactly how the mechanical properties of PNIPAM are affected by a reduction in size. It was recently shown that the swelling behavior of nanopatterned thermoresponsive polymer brushes is strongly dependent on the size of the nanobrushes.[21] It is to be expected that similar size-effects could occur in other types of nanostructures made of stimuli-responsive polymers. However, very little work has been devoted to the nanomechanical properties of PNIPAM-based systems with submicrometer dimensions. Indeed, the elastic properties have only been measured above and below the LCST for either PNIPAM gel surfaces or for PNIPAM microgel particles.[22–24] The elastic properties of these PNIPAM microparticles have only been determined for the two extreme swollen/shrunken states from AFM force−indentation curves.[23,24]

In the present work, we report on our study of changes in the swelling ratio and the mechanical properties of nanoribbons of a poly(*N*-isopropylacrylamide)-*block*-poly(ethylene terephthalate) (PNIPAM-*b*-PET) diblock copolymer, probed by AFM across the LCST, depending on the polymer chain length. From the analysis of AFM images, the elastic modulus variation of individual nanoribbons was estimated as a function of temperature, which varied between 28 and 44 °C. No direct force

* Corresponding author. Address: Institut des Matériaux Jean Rouxel (IMN), Université de Nantes, 2, Rue de la Houssinière, 44322 Nantes cedex 3, France. E-mail: sadia.radji@yahoo.fr. Phone: ++33 240376421. Fax: ++33 240373991.

† Université de Nantes.

‡ Nancy Université.

§ Université Catholique de Louvain.

10.1021/jp909819h
Published on Web 03/16/2010

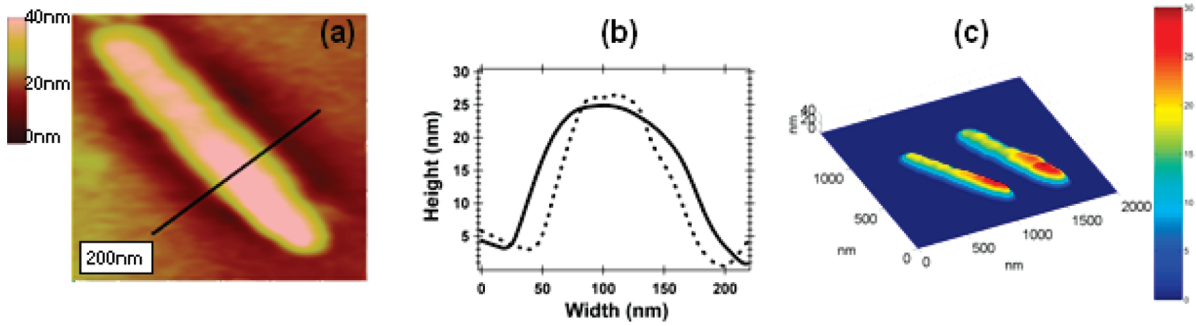

Figure 1. (a) Contact-mode AFM image of a 4h-nanoribbon in water at 44 °C. The solid line represents the location of the cross-section for panel b. (b) Two cross sections realized on the same 4h-nanoribbon at 28 °C (solid line) and 44 °C (dashed line). (c) Numerical reconstruction of the nanoribbon shape at 44 °C (left) and 28 °C (right).

measurement was performed. To achieve this aim, we probed at nanoscale for the first time the elastic properties of the same individual nanoribbon submitted to an external stimulus. Depending on both temperature and polymerization time, the elastic properties of nanoribbons spanned several orders of magnitude. Because of the synthesis in a confined medium, the elastic modulus values of the nanoribbons were found to depend on the degree of confinement during synthesis. Importantly, our approach to evaluate elastic properties based on AFM imaging and the total energy minimization of the investigated system is of interest for other soft micro- and nanosystems such as "fragile" cells.

2. Experimental Methods

Synthesis of the PNIPAM-*b*-PET Nanoribbons. PET track-etched membranes with a thickness of 21 μm, pore size of 80 nm, and pore density of 8×10^8 pores cm^{-2}, were supplied by It4ip, Seneffe, Belgium (http://www.it4ip.be). The nanoporous membranes were obtained by heavy-ion irradiation of PET films in a cyclotron, followed by the chemical development of the latent traces in an hydrolytic bath.[25] The water used in all experiments was purified by a Millipore system (Milli-Q water of 18 MΩ × cm resistivity). *N*-isopropylacrylamide (NIPAM, ACROS) was dissolved in dichloromethane and purified by two extractions with an aqueous sodium hydroxide (NaOH) solution (0.1M) followed by two extractions with Milli-Q water and by drying over anhydrous sodium sulfate (Na_2SO_4) before polymerization. The membranes were immersed for 24 h in a solution containing 0.5 M 2-bromo-2-methylpropanoyl bromide (BMBP, ACROS) and 5 M pyridine (ACROS) in tetrahydrofuran (THF). The reaction between the alcohol groups of PET and BMPB yielded 2-bromo-2-methyl-propanoate groups grafted on the membrane surfaces and nanopore walls. THF was filtered through the pores, and the membranes were copiously rinsed with THF and then dried under a nitrogen gas stream. The bromo-derivatized samples were placed under vacuum for 24 h prior to NIPAM polymerization. Each sample was placed in a deoxygenated Schlenk tube, and a degassed mixture of NIPAM (10 g in 30 mL of Milli-Q water) was transferred into the reactor. A degassed aqueous solution (20 mL) of CuBr (0.1 M, ACROS), $CuBr_2$ (0.05 M, ACROS), and 2,2′-bipyridine (biPy 0.3 M, ACROS) was then transferred into the Schlenk tube, and polymerization was carried out at 20 °C under a nitrogen atmosphere for 4 or 21 h. This synthesis method is the surface-initiated atom transfer radical polymerization (ATRP) method. After polymerization, the samples were washed by immersion in water at ambient temperature and filtration of water through the nanopores. The samples were dried under a nitrogen gas stream and placed under vacuum for 24 h prior to the release of PNIPAM-*b*-PET nanoribbons. For AFM imaging and measurements, the PET membranes were dissolved in pentafluorophenol (PFP, ACROS) and the freed PNIPAM-*b*-PET nanoribbons were collected onto a flat substrate.

AFM Experiments. AFM experiments were carried out with a Multimode Nanoscope IIIA (Veeco-Digital Instruments, Santa Barbara, CA) equipped with a fluid cell and with a temperature accessory. The microscope was equipped with a *J* scanner (100 × 100 μm^2 $x-y$ scan size). To image the nanoribbons, the contact mode was employed in milli-Q water while varying the temperature from 28 to 44 °C by steps of 2 °C. Silicon nitride cantilevers having a nominal spring constant of 0.05 N/m were used to image nanoribbons and to perform force spectroscopy measurements. For these experiments, force curves were recorded with a loading rate of 25 nN/s in Milli-Q water at 10 °C.

3. Results and Discussion

PNIPAM-*b*-PET nanoribbons were synthesized using the template-based method reported previously.[25] Briefly, PNIPAM brushes were grown from the walls of the nanopores of PET track-etched membranes (pores diameter of 80 nm) by surface-initiated ATRP. In this study, the polymerization was carried out either for 4 or 21 h, corresponding to different PNIPAM chain lengths. Generally, varying confinement in a template method is equivalent to varying the diameter of the pores. In our case, the conditions of confinement were modified by varying the chains length for a given pore diameter. Each PNIPAM chain grows from an initiator group linked to a PET chain end created by the irradiation and hydrolysis steps. Thus, the resulting polymer is essentially composed of PNIPAM-*b*-PET diblock copolymer chains, where the PET segment is of variable length due to the statistical nature of the PET chain scission process. The PNIPAM-*b*-PET nanoribbons were then liberated from the template thanks to dissolution of the PET membrane in PFP. When the nanotubes were brought in contact with a surface, their initial perfectly cylindrical shape within the membrane pores was replaced by a flattened shape referred to as a "ribbon" in this study. For this point, we will refer to PNIPAM-*b*-PET nanotubes synthesized for a duration of 4 or 21 h and deposited on a flat surface as "4h-nanoribbons" or "21h-nanoribbons".

Nanoribbons obtained for both synthesis times were analyzed from AFM images taken at different temperatures in water. Figure 1a is an AFM image showing the shape of a nanoribbon at 44 °C. For each temperature, the AFM images correspond to the equilibrium state of the nanoribbon−water system. A cross-section is extracted from AFM images of one nanoribbon at two extreme temperatures (28 °C, 44 °C) at the same location

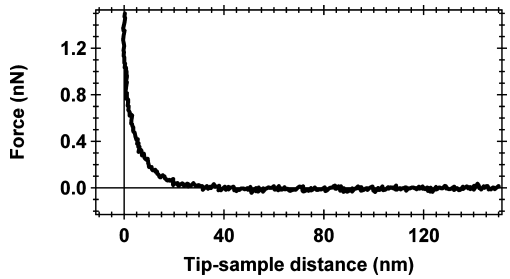

Figure 2. Approach profile of a force curve obtained on a nanoribbon (in water at 28 °C) showing a compression profile typical of a swollen polymer brush under compression.

(Figure 1b). The 28 °C cross-section has a larger width than that obtained at 44 °C, indicating that the shape of the nanoribbons changes with temperature. Indeed, at 28 °C, the PNIPAM portion of the nanoribbons is in a swollen state, whereas at 44 °C it is in a collapsed state. In Figure 1c, the same nanoribbon is numerically reconstructed in three dimensions for these two temperatures. In this three-dimensional (3D) representation, it can be seen that the nanoribbon swells along its whole length when the temperature decreases. Hence, by varying the temperature, the nanoribbon shape changes as well as its volume. As PET chains are not water-soluble, the volume change of nanoribbons comes exclusively from the swelling of the PNIPAM block.

One could thus wonder about the spatial localization of the PET segments. AFM force−distance curves were used to answer this question. It was found that only about 50% of force curves realized along several nanoribbons present the monotonically increasing compression profile typical for a polymer brush swollen in a good solvent (Figure 2).[26] Therefore, the nanoribbon structure is heterogeneous along its length, with PNIPAM chains either in brushes or in network-like portions of the nanoribbons. Despite this heterogeneous local structure, the fact that the nanoribbons swell uniformly along their whole length (Figure 1) indicates that the influence of their detailed structure is irrelevant with respect to the swelling of PNIPAM. In a previous work, the structure of these nanoribbons was determined from AFM force spectroscopy measurements.[27]

The PNIPAM-*b*-PET nanoribbons thus show the same swelling behavior as macroscopic PNIPAM gels or PNIPAM microgel particles.[22–24,28] In the present case, the PET blocks act as a physical cross-linker, whereas the PNIPAM blocks provide thermoresponsiveness. At temperatures below the LCST, intermolecular hydrogen bonds between water molecules and PNIPAM chains become predominant. In this case, the hydrophilicity of PNIPAM induces the swelling of nanoribbons. In contrast, above the LCST, intramolecular hydrogen bonding between groups in PNIPAM chains are favored.[14–16,29] At these temperatures, the chains are in a hydrophobic state, resulting in a collapsed shape of nanoribbons.

The swelling behavior of these nanoribbons was described by the Flory−Rehner theory, which is well adapted to neutral gels such as PNIPAM.[30] The total energy of the system (nanoribbon and solvent) is the result of mixing free energy and elastic energy. The shape taken by the nanoribbons at each temperature corresponds to the equilibrium between the mixing osmotic pressure Π_{osm} and the elastic pressure Π_{elas} of the physically cross-linked PNIPAM. At equilibrium, the total energy is minimized so that

$$\Pi_{elas} + \Pi_{osm} = 0 \qquad (1)$$

The expression of the osmotic pressure takes the following form:[30]

$$\Pi_{osm} = -\frac{k_B T N_A}{V_{mol}}(\ln(1-\phi) + \phi + \chi_{12}\phi^2) \qquad (2)$$

where k_B is the Boltzmann constant, T is the absolute temperature, N_A is Avogadro's number, ϕ is the volume fraction of the polymer, V_{mol} is the water molar volume, and χ_{12} is the solvent−polymer interaction parameter. The expression of χ_{12} is given by[30]

$$\chi_{12} = \frac{\Delta H - T\Delta S}{k_B T} + \chi_2\phi + \chi_3\phi^2 \qquad (3)$$

ΔS is the entropic energy change, and ΔH represents the enthalpic energy change upon mixing. These variations reflect the difference per solvent molecule when a solvent−solvent interaction is replaced by a polymer−solvent interaction. The first term of χ_{12} is the original Flory interaction parameter, whereas χ_2 and χ_3 correspond to independent temperature parameters.

As nanoribbons were adsorbed to a flat substrate, their swelling was considered in two dimensions (Figure 1) for the calculation of the elastic pressure:[30]

$$\Pi_{elas} = -\frac{k_B T\phi}{N_r}\left(\frac{\phi_0}{\phi} - \frac{1}{2}\right) \qquad (4)$$

where ϕ_0 is the volume fraction of the polymer at 44 °C, and N_r the volume occupied by the polymer segments between two neighboring physical cross-linking points.

As previously shown, the volume of nanoribbons increases when the temperature decreases. The nanoribbons volume is V_0 at 44 °C and V for the other temperatures. The swelling ratio, which is defined as $Q = V/V_0$, is related to the temperature by the following equation, obtained by combining the four previous equations:

$$\frac{1}{T} = \frac{\Delta S}{\Delta H} + \frac{k_B}{\Delta H}\left[-\chi_2\phi_0 Q^{-1} - \chi_3\phi_0{}^2 Q^{-2} + \left(\frac{V_{mol}}{2N_A N_r} - 1\right)\frac{Q}{\phi_0} - \left(\frac{V_{mol}}{N_A N_r} + \frac{1}{\phi_0}\ln\left(1 - \frac{\phi_0}{Q}\right)\right)\frac{Q^2}{\phi_0}\right] \qquad (5)$$

The temperature dependence of eq 5 comes explicitly from the original Flory interaction parameter, which plays a key role in the swelling thermodynamics of nanoribbons. For each temperature, the volume of the nanoribbon was extracted numerically from the AFM images (Figure 1c). From these data, the swelling ratio was calculated for each temperature and is reported in Figure 3.

The uncertainty on the swelling ratio comes from the error on the numerical volume. The swelling ratio increases with decreasing temperature up to a threshold corresponding to the maximum Q value. For seven nanoribbons synthesized for 4 h, the average maximum Q value is 1.9 ± 0.2. This value is about 2 for 4h-nanoribbon, meaning that the nanoribbon volume at lower temperature is twice that obtained at higher temperature. For six nanoribbons synthesized for 21 h, the average maximum Q value is 1.2 ± 0.1. The experimental dispersion of the

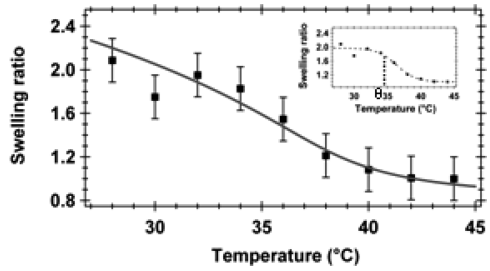

Figure 3. Experimental swelling ratio for a 4h-nanoribbon as a function of temperature (squares). The solid curve corresponds to the theoretical fit. The inset shows the determination of the volume phase transition temperature (VPT) for a 4h-nanoribbon.

TABLE 1: Fitting Parameters Values Obtained for 4h-Nanoribbon and 21h-Nanoribbon

	4h-nanoribbon	21h-nanoribbon
N_r (m^3)	35.10^{-29}	3.10^{-29}
ΔS (J/K/mol)	$-4.4.10^{-22}$	-5.10^{-22}
ΔH (J/mol)	$-1.36.10^{-19}$	$-1.54.10^{-19}$
ϕ_0	0.82	0.96
χ_2	0.1	0.23
χ_3	0.2	0.2

maximum Q values measured for several nanoribbons, for both polymerization times is about 10%.

In the inset of Figure 3, the experimental data of the swelling ratio as a function of the temperature ($Q-T$ data) are fitted by a sigmoid in order to determine the exact volume phase transition (VPT) temperature value (θ). This temperature of the PNIPAM−water system corresponds to the temperature at which the excluded volume is zero. The VPT temperature experimental values are equal to 35 and 36.5 °C, for the 21h-nanoribbon and 4h-nanoribbon, respectively. These results are in good concordance with the well-known LCST value of PNIPAM chains, which is around 32 °C.[31] Moreover, recent experimental works performed on PNIPAM microparticles indicate that the VPT temperature is located between 32 and 34 °C.[24,32]

In Figure 3, the $Q-T$ experimental data were fitted with the theoretical equation (eq 5) determined previously. At the VPT temperature, the Flory interaction parameter is equal to 0.5, allowing one to express ΔH as a function of ΔS and θ. Different fits were tested by adjusting the following parameters: N_r, ΔS, χ_2, χ_3 and ϕ_0. Restrictive conditions are associated with these different parameters. ΔS has to be negative, and ϕ_0 should be positive and slightly lower than 1. For temperatures lower than θ, χ_{12} has to be below 0.5 and the χ_2 value has to be lower than 1/3. χ_2, χ_3, and ΔS are interaction parameters related to the PNIPAM−water system, whereas N_r and ϕ_0 are intrinsic parameters of the block copolymer nanoribbon structure. A good concordance between the experimental results and the theoretical dependence of Q with the temperature could be obtained (Figure 3). The parameter values corresponding to the best fit are reported in Table 1.

The ΔS values are negative for each sample, as expected for a polymer having a LCST like that of PNIPAM. Moreover, as ΔS is an intrinsic parameter of the polymer−solvent system, comparable ΔS values are obtained for both samples. The resulting values of ΔH are in good concordance with values obtained by other authors.[33] To properly describe the discontinuous phase transition occurring in the PNIPAM−water system, ϕ corrections have to be introduced in the χ_{12} parameter (eq 3). As expected, the determined χ_2 values are lower than 1/3, which represents the theoretical critical value predicted for a gel with infinitely long chains.[34]

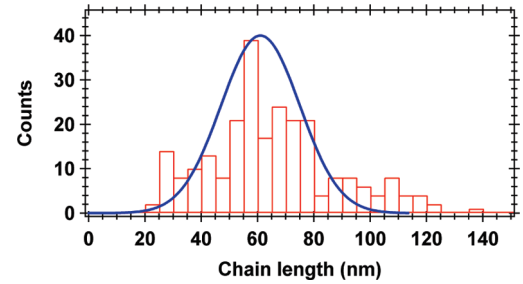

Figure 4. Distribution of the rupture lengths measured from force spectroscopy experiments realized on several 21h-nanoribbons in water.

Table 1 indicates that the value of N_r corresponding to 21h-nanoribbons is much lower than that corresponding to the 4h-nanoribbons. This result indicates that the cross-linking density is larger for nanoribbons synthesized for 21 h than for those synthesized for 4 h. The cross-linking of the PNIPAM chains is due to different factors: PET blocks acting as physical cross-links, irreversibly trapped entanglements, and chemical cross-links arising from uncontrolled radical reactions. Whereas the first cross-links are identical in type and number in the two types of nanoribbons, the two other cross-links may be different. This is because the synthesis of the PNIPAM chains occurs in a very tight environment of diameter close to the PNIPAM chain lengths, where the probability to observe cross-reactions or entanglement trapping may be strongly dependent on chain length. Uncontrolled radical reactions cannot be excluded due to the difficulty to polymerize NIPAM by ATRP (the monomer tends to interfere with the ligand−Cu complex). AFM force spectroscopy measurements realized on the investigated nanoribbons were analyzed to extract the rupture length of PNIPAM chains at 10 °C in water. Figure 4 presents the distribution of the 250 measured rupture lengths for 21h-nanoribbons. The most probable length is centered on 37 ± 9 and 61 ± 14 nm, respectively, for 4h- and 21h-nanoribbons. To obtain the contour length of the chains, these rupture lengths should be corrected by an extension ratio. This ratio is typically determined by fitting the retraction curves to a statistical mechanical ideal chain model, such as the wormlike chain or freely jointed chain models. Several works realized on different polymers have shown that the chains can be stretched to about 94% of their contour length.[26] Therefore, by taking into account this ratio, the contour length can be deduced as 39 ± 9 nm (4h-nanoribbons) and 64 ± 14 nm (21h-nanoribbons). So the conditions of confinement were modified by varying the chain lengths for a pore diameter of 80 nm. The observed decrease of N_r by a factor of 10 when increasing the polymerization time suggests that the much more crowded PNIPAM chains of the 21h-nanoribbon have either irreversibly trapped a large number of entanglements, due to confinement, or have cross-reacted when approaching each other upon filling the nanopores. At any rate, Table 1 indicates that the physical or chemical cross-linking density increases significantly with the ratio between the chain length and the pore diameter.

This conclusion is also supported by the consideration of ϕ_0, which corresponds to the volume fraction of polymer at 44 °C when the nanoribbons are in a collapsed state. In this state, the chains are hydrophobic, and few solvent molecules are incorporated in the nanoribbons. In the ideal case of very dense polymer network, ϕ_0 tends to 1. For 4h-nanoribbons, there are about 20% of water molecules contained within the collapsed nanoribbons, whereas only 4% remain in the 21h-nanoribbons. The higher value of ϕ_0 for 21h-nanoribbons indicates a lower

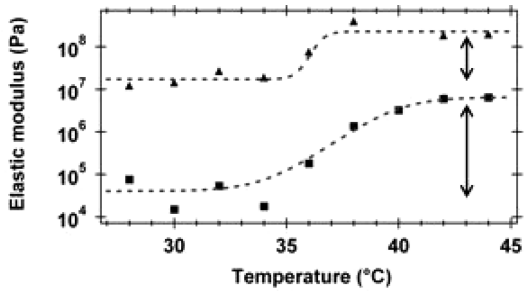

Figure 5. Experimental evolution of the elastic modulus of the PNIPAM blocks as a function of temperature for a 4h-nanoribbon (square) and for a 21h-nanoribbon (triangle). Arrows represent the range in which the elastic modulus values vary for both samples.

propensity to swell in the collapsed state, which is well in line with its higher cross-linking density. Hence, the thermodynamic theory of Flory−Rehner is able to properly describe the swelling of PNIPAM-*b*-PET nanoribbons as a function of temperature, with a set of consistent parameters.

During the swelling, as the structure of the nanoribbons varies, their elastic properties should be modified. In a previous work, the authors used the electrostatic resonant contact method to measure the elastic modulus of polyelectrolyte nanotubes,[35] using nanotubes suspended above the pores of a membrane. Such a configuration cannot be taken for the softer PNIPAM nanoribbons, which plunge into the pores if suspended over their length. Therefore, the elastic modulus values were extracted from the deformed shape of nanoribbons. The shear modulus of nanoribbons is defined as the absolute value of the elastic pressure (eq 4). By taking into account the experimental data of the swelling ratio (Figure 3) and the different fitting parameters previously determined (Table 1), the elastic modulus was computed as a function of temperature for each sample (Figure 5). From the classical theory of rubberlike elastic networks, the elastic modulus of cross-linked polymer networks corresponds to 3 times the shear modulus.[24,36]

Whatever the synthesis time, the profile evolution of the elastic modulus with temperature is the same: the elastic modulus increases when the temperature increases due to water expulsion. More importantly, whatever the temperature, the elastic modulus values are much larger for 21h-nanoribbons than those obtained for 4h-nanoribbons. Since the elastic modulus directly reflects the cross-linking density, the conclusion follows again that this density is higher for 21h-nanoribbons. This supports our argument that the nanoconfinement induces more cross-linking in the PNIPAM chains, for chemical or physical reasons. For 21h-nanoribbon, the highest elastic modulus value is around 200 MPa whereas for 4h-nanoribbon, this value is around 7 MPa. The transition from the swollen state (28 °C) to the collapsed state (44 °C) induces a variation of the elastic modulus of 1 order of magnitude for 21h-nanoribbons, versus 2 orders of magnitude for the 4h-nanoribbons.

The elastic modulus values of the 4h-nanoribbons are close to those measured for PNIPAM microgel particles or for PNIPAM gel surfaces: Tagit et al. determined 1.8 and 12.8 MPa for the two extreme states of microgel particles, whereas Matzelle et al. estimated the elastic modulus of PNIPAM surfaces to be below 1 MPa.[22,24] The elastic modulus of water-swollen brushes of a closely related neutral water-soluble polymer, poly(oligo(ethylene glycol) methacrylate), was determined by quartz-crystal microbalance measurements with dissipation monitoring to be $\sim 10^5$ Pa.[37] The range of thermal variations observed for the 4h-nanoribbons is also in good concordance with those observed for PNIPAM gel surfaces and microparticles. AFM indentation measurements performed on gel surfaces indicated a variation of elastic modulus by 2 orders of magnitude between the two extreme temperatures.[22] PNIPAM particles of elasticity differing by a 10−15-fold factor between the swollen and collapsed states have also been reported in the literature.[23,24] This shows that the PNIPAM chains in the 4h-nanoribbons behave essentially as expected for a lightly cross-linked PNIPAM gel of a dense brush. Furthermore, these observations show that the influence of PET segments on the elasticity of the PNIPAM chains is limited (note that this may not be the case for the whole nanoribbon). In contrast, the elastic moduli of the 21h-nanoribbon are much larger than expected. This again may only arise from a much larger cross-linking density, which by necessity must result from the strong confinement of the 64 nm-long chains in the 80 nm-diameter nanopores. Whether this is due to chemical or physical factors, or both, remains to be decided.

4. Conclusion

In conclusion, we have evaluated the elastic modulus of PNIPAM-*b*-PET nanoribbons as a function of temperature. Such responsive polymer nanomaterials swell increasingly with decreasing temperature. For each temperature, the volume of nanoribbons was numerically extracted from AFM images. A good concordance was obtained between the experimental swelling ratio and the calculated curve coming from the thermodynamic theory of swelling. The elastic modulus was estimated using a novel approach based on AFM images, without measuring forces. A similar approach could be particularly well-suited to the in situ study of elastic properties of "fragile" proteins or living cells evolving in time. Here, the elastic modulus variation of individual nanoribbons depending on both temperature and polymerization time (confinement conditions) was estimated. Whereas the elastic modulus is close to the values reported for PNIPAM gels and brushes for nanoribbons with a short polymerization time, the values obtained deviate significantly from the expected ones for longer polymerization times. This is caused by a strongly increased cross-linking density, arising either from trapped entanglement or chemical cross-links generated when the PNIPAM chains reach a length comparable to the diameter of the nanopores. This indicates that severe nanoconfinement results in important changes in the morphology and growth of grafted brushes. Therefore, simply by playing with the confinement condition of responsive polymer nanoribbons, their elastic modulus can be varied over several orders of magnitude. In the future, a new class of nano-objects made of responsive polymers could thus be processed with adjustable physical properties under external stimuli.

Acknowledgment. S.C. acknowledges the "Agence Nationale de la Recherche" for financial support in the frame of the "ANR06-Jeunes Chercheurs-n°24" program. We thank Etienne Ferain and the It4ip company for supplying PET membranes. The work was supported by the Belgian Science Policy through the Interuniversity Attraction Pole Programs (P6/27 and P6/42). S.D.-C. thanks the F.R.S.-FNRS for her Senior Research Associate position.

Note Added after ASAP Publication. This paper was published ASAP on March 16, 2010. An author name was revised. The updated paper was reposted on March 25, 2010.

References and Notes

(1) Salvetat-Delmotte, J.-P.; Rubio, A. *Carbon* **2002**, *40*, 1729.
(2) Dai, H. J. *Acc. Chem. Res.* **2002**, *35*, 1035.
(3) Wang, J. F.; Gudiksen, M. S.; Duan, X. F.; Cui, Y.; Lieber, C. M. *Science* **2001**, *293*, 1455.
(4) Falvo, M. R.; Clary, G. J.; Taylor, II, R. M.; Chi, V.; Brooks, Jr, F. P.; Washburn, S.; Superfine, R. *Nature* **1997**, *389*, 582.
(5) Yu, M.-F.; Lourie, O.; Dyer, M. J.; Moloni, K.; Kelly, T. F.; Ruoff, R. S. *Science* **2000**, *287*, 637.
(6) Salvetat, J.-P.; Briggs, G. A. D.; Bonard, J.-M.; Bacsa, R. R.; Kulik, A. J.; Stöckli, T.; Burnham, N. A.; Forro, L. *Phys. Rev. Lett.* **1999**, *82*, 944.
(7) Wong, E. W.; Sheehan, P. E.; Lieber, C. M. *Science* **1997**, *277*, 1971.
(8) McDowell, M. T.; Leach, A. M.; Gall, K. *Nano Lett.* **2008**, *8*, 3613.
(9) Cuenot, S.; Frétigny, C.; Demoustier-Champagne, S.; Nysten, B. *J. Appl. Phys.* **2003**, *93*, 5650.
(10) Cuenot, S.; Demoustier-Champagne, S.; Nysten, B. *Phys. Rev. Lett.* **2000**, *85*, 1690.
(11) Li, Y.; Tanaka, T. *J. Chem. Phys.* **1990**, *92*, 1365.
(12) Moselhy, J.; Wu, X. Y.; Nicholov, R.; Kodaria, K. *J. Biomater. Sci. Polym. Ed.* **2000**, *11*, 123.
(13) Tanaka, T.; Nishio, I.; Sun, S. T.; Ueno-Nishio, S. *Science* **1982**, *218*, 467.
(14) Schild, H. G. *Prog. Polym. Sci.* **1992**, *17*, 163.
(15) Pelton, R. *Adv. Colloid Interface Sci.* **2000**, *85*, 1.
(16) Zhang, X. Z.; Wang, F. J.; Chu, C. C. *J. Mater. Sci.: Mater. Med.* **2003**, *14*, 451.
(17) Weissman, J. M.; Sunkara, H. B.; Asher, S. A. *Science* **1996**, *274*, 959.
(18) Kanazawa, H.; Sunamoto, T.; Matsushima, Y.; Kikuchi, A.; Okano, T. *Anal. Chem.* **2000**, *72*, 5961.
(19) Monji, N.; Hoffman, S. *Appl. Biochem. Biotechnol.* **1987**, *14*, 107.
(20) Klouda, L.; Mikos, A. G. *Eur. J. Pharm. Biopharm.* **2008**, *68*, 34.
(21) Jonas, A. M.; Hu, Z.; Glinel, K.; Huck, W. T. S. *Nano Lett.* **2008**, *8*, 3819.
(22) Matzelle, T. R.; Ivanov, D. A.; Landwehr, D.; Heinrich, L. A.; Herkt-Bruns, C.; Reichelt, R.; Kruse, N. *J. Phys. Chem. B* **2002**, *106*, 2861.
(23) Wiedemair, J.; Serpe, M. J.; Kim, J.; Masson, J.-F.; Lyon, L. A.; Mizaikoff, B.; Kranz, C. *Langmuir* **2007**, *23*, 130.
(24) Tagit, O.; Tomczak, N.; Vancso, G. J. *Small* **2008**, *4*, 119.
(25) Alem, H.; Duwez, A.-S.; Lussis, P.; Lipnik, P.; Jonas, A. M.; Demoustier-Champagne, S. *J. Membr. Sci.* **2008**, *308*, 75.
(26) Cuenot, S.; Gabriel, S.; Jérôme, R.; Jérôme, C.; Fustin, C.-A.; Jonas, A. M.; Duwez, A.-S. *Macromolecules* **2006**, *39*, 8428.
(27) Radji, S.; Alem, H.; Demoustier-Champagne, S.; Jonas, A. M.; Cuenot, S. Submitted for publication, 2010.
(28) Cui, Y.; Tao, C.; Zheng, S.; He, Q.; Ai, S.; Li, J. *Macromol. Rapid Commun.* **2005**, *26*, 1552.
(29) Sun, T.; Wang, G.; Feng, L.; Liu, B.; Ma, Y.; Jiang, L.; Zhu, D. *Angew. Chem., Int. Ed.* **2004**, *43*, 357.
(30) Flory, P. J. *Principles of Polymer Chemistry*; Cornell University Press: Ithaca, NY, 1963.
(31) Yim, H.; Kent, M. S.; Mendez, S.; Lopez, G. P.; Satija, S.; Seo, Y. *Macromolecules* **2006**, *39*, 3420.
(32) Höfl, S.; Zitzler, L.; Hellweg, T.; Herminghaus, S.; Mugele, F. *Polymer* **2007**, *48*, 245.
(33) Hirotsu, S.; Hirokawa, Y.; Tanaka, T. *J. Chem. Phys.* **1987**, *87*, 1392.
(34) Erman, B.; Flory, P. J. *Macromolecules* **1986**, *19*, 2342.
(35) Cuenot, S.; Alem, H.; Louarn, G.; Demoustier-Champagne, S.; Jonas, A. M. *Eur. Phys. J. E* **2008**, *25*, 343.
(36) Treloar, L. R. G. *The Physics of Rubber Elasticity*, 3rd ed.; Oxford Clarendon Press: Oxford, U.K., 1975.
(37) Fu, L.; Chen, X.; He, J.; Xiong, C.; Ma, H. *Langmuir* **2008**, *24*, 6100.

JP909819H